Conformational Stability of Inositol 1,3,4,5,6-Pentakisphosphate 2-Kinase (IPK1) Dictates Its Substrate Selectivity*

Varin Gosein[‡] **and Gregory J. Miller**[‡§¶1]

From the ‡*Department of Pharmacology and Therapeutics, McGill University, Montréal, Quebec H3G 1Y6, Canada, the* §*Groupe de Recherche Axé sur la Structure des Protéines, McGill University, Montréal, Quebec H3G 0B1, Canada, and the* ¶*Department of Chemistry, The Catholic University of America, Washington, D. C. 20064*

Background: The phosphate profile of the inositol phosphate (IP) substrate defines inositol 1,3,4,5,6-pentakisphosphate 2-kinase (IPK1) specificity.
Results: IP substrate specificity is linked to IPK1 stability.
Conclusion: IPK1 employs a mechanism of IP-induced stabilization to selectively recognize IP_5.
Significance: The IP recognition mechanism of IPK1 can be exploited to selectively target IPK1 for the study of higher IPs.

Inositol 1,3,4,5,6-pentakisphosphate 2-kinase (IPK1) converts inositol 1,3,4,5,6-pentakisphosphate(IP_5) to inositol hexakisphosphate (IP_6). IPK1 shares structural similarity with protein kinases and is suspected to employ a similar mechanism of activation. Previous studies revealed roles for the 1- and 3-phosphates of IP_5 in IPK1 activation and revealed that the N-lobe of IPK1 is unstable in the absence of inositol phosphate (IP). Here, we demonstrate the link between IPK1 substrate specificity and the stability of its N-lobe. Limited proteolysis of IPK1 revealed that N-lobe stability is dependent on the presence of the 1-phosphate of the substrate, whereas overall stability of IPK1 was increased in ternary complexes with nucleotide and IPs possessing 1- and 3-phosphates that engage the N-lobe of IPK1. Thus, the 1- and 3-phosphates possess dual roles in both IPK1 activation and IPK1 stability. To test whether kinase stability directly contributed to substrate selectivity of the kinase, we engineered IPK1 mutants with disulfide bonds that artificially stabilized the N-lobe in an IP-independent manner thereby mimicking its substrate-bound state in the absence of IP. IPK1 E82C/S142C exhibited a DTT-sensitive 5-fold increase in k_{cat} for 3,4,5,6-inositol tetrakisphosphate (3,4,5,6-IP_4) as compared with wild-type IPK1. The crystal structure of the IPK1 E82C/S142C mutant confirmed the presence of the disulfide bond and revealed a small shift in the N-lobe. Finally, we determined that IPK1 E82C/S142C is substantially more stable than wild-type IPK1 under nonreducing conditions, revealing that increased stability of IPK1 E82C/S142C correlates with changes in substrate specificity by allowing IPs lacking the stabilizing 1-phosphate to be used. Taken together, our results show that IPK1 substrate selection is linked to the ability of each potential substrate to stabilize IPK1.

Inositol 1,3,4,5,6-pentakisphosphate 2-kinase (IPK1,[2] IP_5 2-K) is an inositol phosphate kinase (IPK) that catalyzes the phosphorylation of inositol 1,3,4,5,6-pentakisphosphate (IP_5) to inositol hexakisphosphate (IP_6) (1). IP_6 is involved in diverse cellular processes such as mRNA export (2), chromatin remodeling (3), apoptosis (4), and development (5). IPK1 itself has been demonstrated to affect apoptosis, and its expression is markedly elevated in renal samples from patients suffering from diabetic nephropathy, indicating that it may play functional roles in disease states (6, 7). Recent crystal structures have revealed that some IPKs possess an N- and C-lobed structure similar to that of protein kinases (PKs), in which both lobes contribute to a conserved ATP binding pocket (8). Both PKs and IPKs require mechanisms to recognize their physiological substrates from among pools of similar molecules. Although PKs recognize consensus sequences in their targets, IPKs must recognize their substrates from among more than 30 IPs based on differences in stereochemistry and numbers and patterns of phosphate groups (9, 10). This mechanism must be able to differentiate physiological substrates from non-substrates that may differ by the presence, absence, or position of a single phosphate. Structures of inositol 1,4,5-trisphosphate 3-kinase (IP3K), inositol polyphosphate multikinase (IPMK), inositol 1,3,4-trisphosphate 5/6-kinase/inositol 3,4,5,6-tetrakisphosphate 1-kinase (ITPK1), and diphosphoinositol pentakisphosphate kinase ($PPIP_5K$) all reveal mechanisms that define substrate specificity (11–14). The first crystal structures of IPK1 revealed how IP_5 is phosphorylated on the 2'-hydroxyl of the inositol ring to yield IP_6, but the recognition of all five phosphate groups and the axial hydroxyl group did not offer explanations for how it excludes IPs with fewer than five phosphates from its pool of potential substrates (1, 15). For PKs, the stability of the N- and C-lobes is a critical precursor for kinase activation (16–18), and these IPK1 structures indicated that a similar mechanism might be employed for some IPKs. Comparison

---

[1] To whom correspondence should be addressed: Dept. of Chemistry, The Catholic University of America, Washington, DC 20064. Tel.: 202-319-4766; Fax: 202-319-5381; E-mail: millergj@cua.edu.

[2] The abbreviations used are: IP, inositol phosphate; IPK, inositol phosphate kinase; IPK1, inositol 1,3,4,5,6-pentakisphosphate 2-kinase; PK, protein kinase; IP_4, inositol tetrakisphosphate; IP_5, inositol 1,3,4,5,6-pentakisphosphate; IP_6, inositol 1,2,3,4,5,6-hexakisphosphate; DSF, differential scanning fluorometry; AMPPNP, adenosine 5'-(β,γ-imido)triphosphate.

of IP-bound and free crystal structures of IPK1 suggested that stabilization of its N-lobe was triggered by IP binding (19); however, this mechanism of IP recognition for IPK1, termed "IP-induced stabilization," has yet to be validated. Recently, we demonstrated that the positions of the phosphates on IPK1 substrates play different roles in directing IP binding to IPK1 and the recognition of IPs as substrates (20).

The aim of our current work is to define the contributions of IP phosphates on IPK1 stabilization and define how this relates to enzyme activation. The results presented here demonstrate that the stable conformation of IPK1 is achieved when IP binding sites in the N-lobe are occupied by the 1- and 3-phosphates of the IP and that substrate specificity of IPK1 can be manipulated through artificial stabilization of the N-lobe in an IP-independent manner.

EXPERIMENTAL PROCEDURES

Ligands—Inositol phosphates (1,3,4,5,6-IP$_5$; 1,3,4,5-IP$_4$; 1,4,5,6-IP$_4$; 1,3,4,6-IP$_4$; 3,4,5,6-IP$_4$) were purchased from Cayman Chemical Company (Ann Arbor, MI). Trypsin, ADP, and IP$_6$ were purchased from Sigma-Aldrich. AMPPNP was purchased from Jena Bioscience (Jena, Germany). ATP was purchased from Fisher. All IPs were dissolved in Tris-HCl (pH 8.0) to a stock concentration of 20 mM and stored at $-20\,°C$ until use.

Limited Proteolysis—IPK1 was purified as described previously (19). Limited proteolysis of IPK1 was performed in 50 mM Tris-HCl (pH 8.0), 150 mM NaCl, and 2.5 mM DTT. 9 μM of purified IPK1 was incubated with 2 mM MgCl$_2$ and 1 mM IP (IP$_4$, IP$_5$, or IP$_6$) with and without nucleotides (AMPPNP, ADP) for 20 min at 4 °C. 0.08 μg of trypsin was then added to each reaction, except the undigested control. The reactions were incubated at 20 °C, and samples were taken at 2, 4, 6, and 8 h. Samples were analyzed by SDS-PAGE, stained with Coomassie Blue, and analyzed as described by Gosein *et al* (19).

Densitometry—Densitometry of IPK1 digestion fragments was performed using ImageJ (21). The Analyze Gel module was used as described in the ImageJ manual. The area was measured for the uncut control fragment where no digestion had occurred, and for the full-length fragment and fragments comprising amino acids 52–451 and 130–451 bands in digested conditions. The areas of the digested fragments were plotted as a percentage of the area of the control band.

Differential Scanning Fluorometry (DSF)—DSF was performed on a Corbett Life Science Rotor-Gene 6000. All reactions were prepared individually in 0.2-ml PCR tubes at a final volume of 50 μl. The reactions consisted of 9 μM of purified IPK1 in 50 mM HEPES (pH 7.5), 5 mM MgCl$_2$, 50 mM NaCl, and 2.5 mM DTT buffer, incubated with 1 mM nucleotide (ADP, AMPPNP) and/or 1 mM IP (IP$_4$, IP$_5$, or IP$_6$) for 5 min on ice. SYPRO Orange (Life Technologies) was then added to 5× under dark conditions. The final dimethyl sulfoxide (DMSO) concentration was 0.1%. A temperature melt was carried out between 28 and 80 °C with 0.15 °C/s increments, and the gain was set to 2. The high resolution melt module was used with an excitation filter of 460 nm and emission filter of 510 nm. Each condition was performed in triplicate. Data were analyzed using the Rotor-Gene software. The first derivative of the raw data was analyzed for peaks, which corresponded to the melting temperature (T_m) of IPK1. DSF was performed similarly using IPK1 E82C/S142C mutant purified in the absence of reducing agents; however, the reactions consisted of IPK1 E82C/S142C incubated with nucleotide and/or IP in the absence or presence of 2.5 mM DTT prior to the DSF run.

Generation of IPK1 Disulfide Mutants—The structure of IPK1 was processed using the Disulfide by Design software to identify pairs of residues that could be mutated to cysteines to form disulfide bonds (22). Cysteine mutants of these residues were generated by site-directed mutagenesis using the QuikChange method (Stratagene) in two subsequent steps. A pET28a vector containing wild-type *Arabidopsis thaliana* IPK1 and a hexahistidine tag was used a template (a generous gift from Dr. C. A. Brearley). All mutations were verified by DNA sequencing.

Activity of IPK1 Disulfide Mutant—IPK1 kinase activity was measured using the Kinase-Glo Max luminescent kinase assay (Promega) as per the manufacturer's instructions. Kinase reactions were performed in 25-μl volumes in black 96-well plates at 25 °C and contained 50 mM HEPES (pH 7.5), 6 mM MgCl$_2$, 50 mM NaCl, and 300 μM ATP. 0.1 μM of each IPK1 mutant, purified in the absence of reducing agents, was tested with 80 μM IP in the presence or absence of 2.5 mM DTT. 25 μl of Kinase-Glo reagent was added to stop the reaction. Luminescence was measured after 20 min on a Berthold Orion II microplate luminometer.

IPK1 E82C/S142C Kinetic Analysis—Initially, 80 μM IP was used, and the amount of IPK1 E82C/S142C enzyme was varied to determine conditions in which product formation was linear over 30 min. Subsequently, an array of reactions with varying concentrations of IP (20, 40, 60, 80, 100, 120, and 140 μM) stopped at various time points (2, 5, 10, 20, and 30 min) was performed in triplicate. The process was performed for both IP$_5$ and 3,4,5,6-IP$_4$, in the absence of reducing agent. The rate of product formation *versus* IP concentration was plotted and fitted to the Michaelis-Menten equation using nonlinear regression to determine K_m and V_{max} (GraphPad). Values were reported as mean $\pm$ S.D. The k_{cat} values were calculated using the equation $k_{cat} = V_{max}/[E]$, where $[E]$ is the concentration of enzyme in μM.

Structure Determination of IPK1 E82C/S142C Mutant—IPK1 E82C/S142C was expressed and purified as described previously for wild-type IPK1; however, DTT and β-mercaptoethanol were omitted in all buffers (19). IPK1 E82C/S142C at 5 mg/ml crystallized with 5 mM ADP/MgCl$_2$, 5 mM IP$_6$ in 0.08 M MES (pH 6.5), 19.85% PEG 3000, 0.17 M NaCl, 2.35% benzamidine HCl at 20 °C within 6–72 h using the sitting-drop vapor diffusion method. X-ray diffraction data were collected on a Rigaku MicroMax-007 HF microfocus x-ray generator fitted with Varimax x-ray optics and a Saturn 944+ CCD detector. Crystals were cryoprotected with reservoir solution that included 10% PEG 400, and data were collected under cryogenic conditions. Diffraction data were analyzed and processed with the HKL2000 software and refined with Phenix and Coot (23–25). Molecular replacement was performed with Protein Data Bank code: 2XAM. All model images were created using PyMOL (27).

RESULTS

Positions of Substrate Phosphates Determine Extent of IPK1 Stabilization—We used limited proteolysis as a probe for IPK1 stability (19). As reported previously (19), IPK1 can be cleaved by trypsin at Arg-130 when the N- and C-lobes are not stabilized, but not when the N- and C-lobes have stabilized (Fig. 1*A*). To identify phosphate groups of the IP substrate that promote IPK1 stabilization, we performed limited proteolysis of IPK1 in complex with IPs alone or in ternary complexes ($AMPPNP+IP_4$, $AMPPNP+IP_5$, or $ADP+IP_6$). The resulting proteolytic patterns observed on SDS gels were compared (Fig. 1*B*). In contrast to IP alone, IPK1 in complex with both nucleotide and IP protected an additional 46-kDa fragment with Lys-52 at its N terminus, indicating that the Arg-130 site was protected under these conditions (Fig. 1*B*). To assess the relative stability of IPK1 in the complexes, we performed densitometry to compare the ratios of the stabilized fragments to uncut IPK1 (Fig. 1*C*). The amounts of full-length fragment in each of the ternary complexes were similar, indicating that digestion occurred to a similar extent in each of these complexes (Fig. 1*C*, *green bars*). There was little variability in the amount of the Arg-130-Ser-451 band between the different complexes, indicating that C-lobe stability was very similar in each of the complexes (Fig. 1*C*, *blue bars*). Finally, the amount of the Lys-52-Ser-451 band varied between each of the ternary complexes, indicating that IPK1 was differentially stabilized specifically at the N-lobe when IPK1 was bound to different IPs (Fig. 1*C*, *red bars*). Protection of the Lys-52 cleavage site is substantially decreased with IPK1 in complex with AMPPNP and $3,4,5,6-IP_4$ as compared with other ternary complexes, which demonstrates that the 1-phosphate of the IP is singularly important for N-lobe stabilization.

To further characterize the overall stability of IPK1, we used DSF to measure the melting point of IPK1 in the ligand-free state, bound to nucleotide (AMPPNP or ADP), bound to IP (IP_4s, IP_5, or IP_6), or as ternary complexes bound to both nucleotide and IP (Fig. 2). In the free state, IPK1 exhibited a T_m of 35 °C. When bound to either AMPPNP or ADP, the T_m of IPK1 increased to 38 °C, indicating that nucleotide contributes to the overall stability of IPK1. When bound to IPs only, except $1,4,5,6-IP_4$, IPK1 exhibited T_m values of 40 °C, revealing that the stability of IPK1 is impacted more by the binding of IP than nucleotide. Finally, in the ternary complexes, IPK1 exhibited varying T_m values that were dependent on the phosphorylation pattern of the IP. When also bound to nucleotide, IPK1 displayed markedly lower T_m values in the $3,4,5,6-IP_4$ and $1,4,5,6-IP_4$ conditions as compared with the $1,3,4,6-IP_4$, $1,3,4,5-IP_4$, IP_5, and IP_6 conditions. Our results indicate that the 1- and 3-phosphate groups contribute more to the overall stability of IPK1 than other phosphates when IPK1 is in the nucleotide-bound state.

IPK1 Disulfide Mutants Alter Specificity—Observing that binding of different IPs led to differential stabilization of IPK1, we hypothesized that IPK1 stabilized in an IP-independent manner would exhibit altered specificity for IP substrates, diminishing the requirement for N-lobe-interacting 1- and 3-phosphates that stabilize IPK1. To test this role of IPK1 sta-
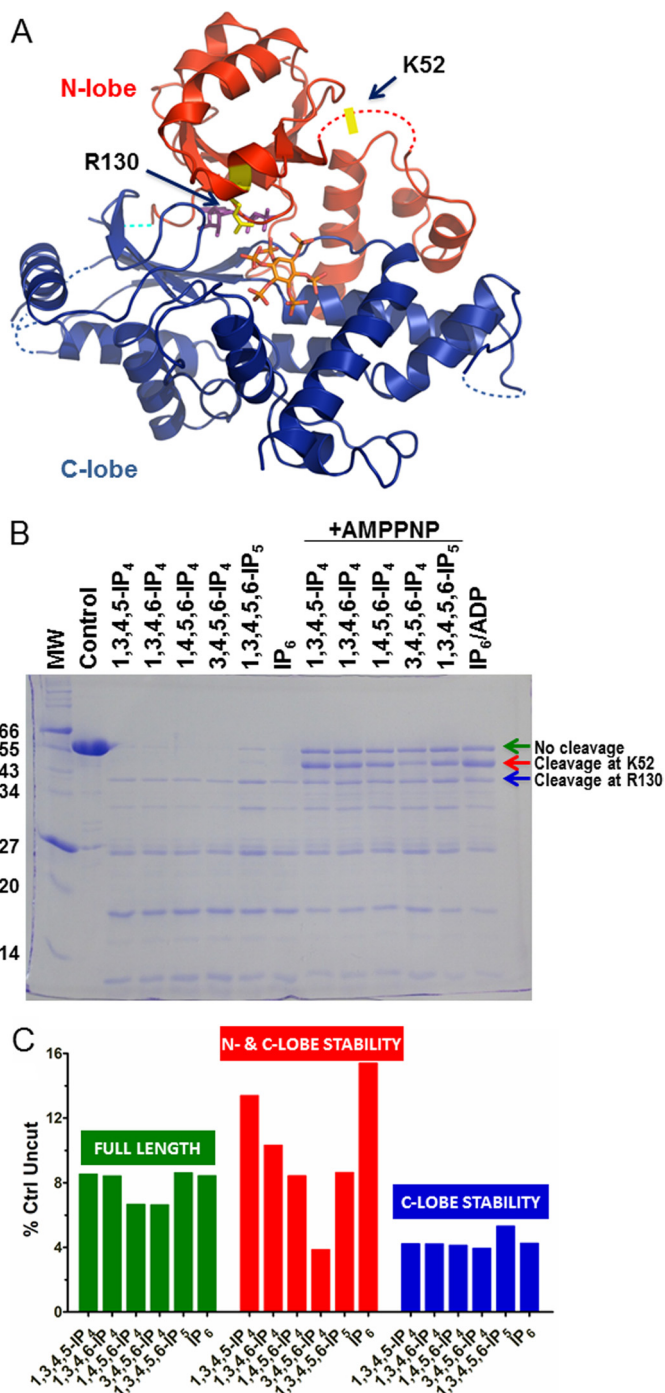

FIGURE 1. **Localized stability of N-lobe with 1-phosphate IPs.** *A*, graphic representation of product-bound IPK1 depicting overall topology: N-lobe (*red*), C-lobe (*blue*), and hinge (*cyan*) with ADP (*purple, stick form*) and IP_6 (*orange, stick form*) (Protein Data Bank code: 3UDZ). *Dashed lies* indicate untraceable regions. *B*, limited proteolysis of IPK1. IPK1 (55 kDa) was incubated with trypsin in the presence of nucleotides and/or inosities. Two fragments were protected in multiple conditions; one fragment cleaved at Lys-52 (46 kDa, *red arrow*), and the other cleaved at Arg-130 (37 kDa, *blue arrow*). Both residues are shown in *yellow* in *A* (Lys-52, *rectangle*; Arg-130, *stick form*). *MW*, molecular weight markers. *C*, densitometry of limited proteolysis gel. The ratios of the stabilized fragments to control (*Ctrl Uncut*) IPK1 were plotted for the full-length band (*green*), the Lys-52 band (*red*), and the Arg-130 band (*blue*) for each ternary complex.

bilization, we engineered and tested a series of disulfide bonds to artificially stabilize the N-lobe of IPK1. We created double cysteine mutants of IPK1 at different sites near residues 110–
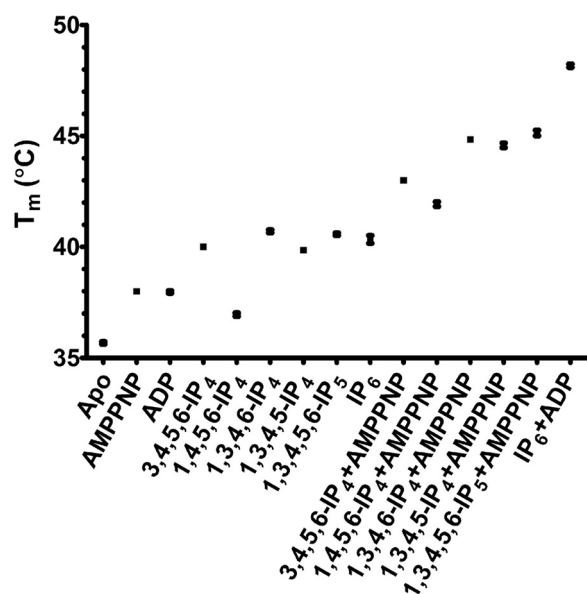
FIGURE 2. **N-lobe binding 1- and 3-phosphates increase the overall stability of IPK1.** The T_m of IPK1 was measured using DSF to determine the overall stability of IPK1 in complex with different nucleotides and/or inositides as shown. Each point represents the mean ± S.D. of triplicate experiments.
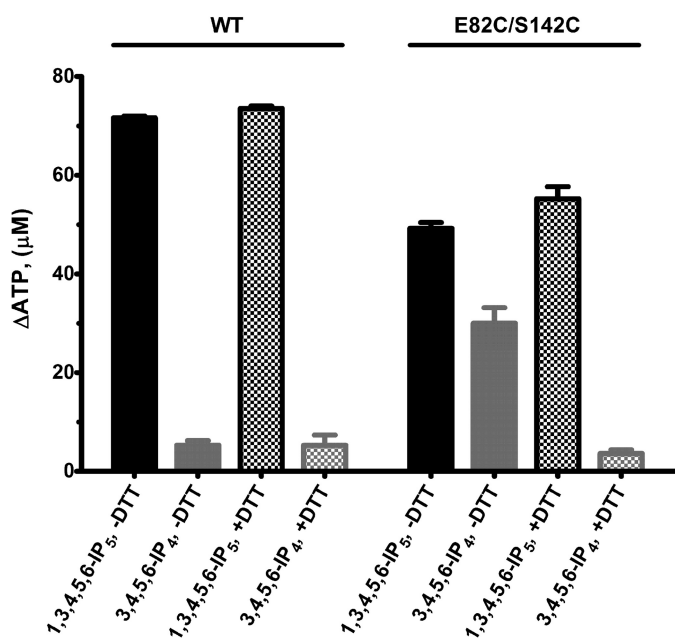

FIGURE 3. **IPK1 E82C/S142C confers specificity to 3,4,5,6-IP4.** Wild-type IPK1 and the disulfide mutant IPK1 E82C/S142C were tested for kinase activity with 1,3,4,5,6-IP$_5$ (*black bars*) or 3,4,5,6-IP$_4$ (*gray bars*), in the absence (*solid*) or presence (*shaded*) of DTT. Each *error bar* represents the mean ± S.D. of triplicate experiments.

140, the region of the N-lobe that was previously observed to be unstable in the absence of IP (19). We tested the kinase activity of these mutants using its physiological substrate, IP$_5$, and 3,4,5,6-IP$_4$, a poor IPK1 substrate (20), in reducing and nonreducing conditions (Fig. 3). Wild-type IPK1 displayed very high activity for IP$_5$ and very low activity for 3,4,5,6-IP$_4$ and was unaffected by DTT. The IPK1 E82C/S142C mutant showed moderate activity for IP$_5$ and greater activity for 3,4,5,6-IP$_4$ than the wild-type enzyme under nonreducing conditions, and wild-type activity was restored in the presence of DTT (Fig. 3).
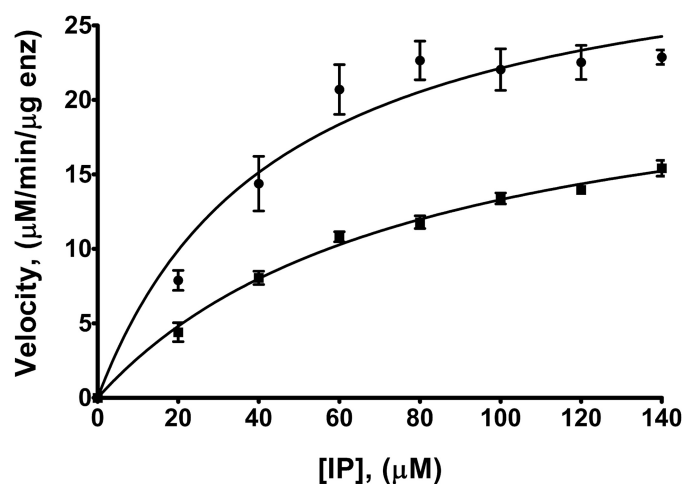

FIGURE 4. **Kinetic analysis of IPK1 E82C/S142C.** Kinase activity of IPK1 E82C/S142C toward 1,3,4,5,6-IP$_5$ or 3,4,5,6-IP$_4$ was assessed in the absence of DTT by plotting the rate of product formation *versus* IP concentration fitted to the Michaelis-Menten equation. Each point represents the mean ± S.D. of triplicate experiments. ●, IPK1 E82C/S142C with 1,3,4,5,6-IP$_5$; ■, IPK1 E82C/S142C with 3,4,5,6-IP$_4$. *enz*, enzyme.

TABLE 1

Kinetic parameters of IPK1 E82C/S142C

Wild-type IPK1 data were previously obtained and are provided for comparison (20). Data represent the mean ± S.D. of triplicate experiments.

IPK1	IP	K_m	k_{cat}	k_{cat}/K_m
		μM	min^{-1}	
Wild-type	3,4,5,6-IP$_4$	47.54 ± 13.94	6.30 ± 0.68	0.13
Wild-type	1,3,4,5,6-IP$_5$	63.05 ± 10.77	44.02 ± 3.19	0.70
E82C/S142C	3,4,5,6-IP$_4$	79.17 ± 8.51	32.93 ± 1.66	0.41
E82C/S142C	1,3,4,5,6-IP$_5$	44.53 ± 13.43	44.18 ± 4.76	0.99

This demonstrated the mutations themselves, which are remote from the active site, are not responsible for the altered activity and that the changes were due primarily to the formation of the disulfide bond.

To further examine the effect of the disulfide bond on IPK1 kinase activity, we performed a kinetic analysis of IPK1 E82C/S142C with IP$_5$ or 3,4,5,6-IP$_4$, under nonreducing conditions (Fig. 4). IPK1 E82C/S142C exhibited similar K_m and k_{cat} values to that of wild-type IPK1 with IP$_5$ as a substrate, both possessing k_{cat} values of ~44 nmol/min (Table 1). In contrast, IPK1 E82C/S142C displayed a 5-fold increase in kinase activity (k_{cat} = 32.93 nmol/min) with 3,4,5,6-IP$_4$ as a substrate as compared with wild-type IPK1 (k_{cat} = 6.30 nmol/min) (Table 1). The ratio of k_{cat}/K_m for the disulfide mutant and wild-type IPK1 for each IP revealed changes in substrate selectivity due to the presence of the disulfide bond. We observed that wild-type IPK1 had a 5.3:1 preference for IP$_5$ over 3,4,5,6-IP$_4$ when comparing IP selectivity. In contrast, IPK1 E82C/S142C displayed a 2.5:1 preference for IP$_5$ over 3,4,5,6-IP$_4$, demonstrating that the disulfide bond altered substrate specificity of IPK1.

IPK1 E82C/S142C Increases Overall Stability of IPK1—To explore structural changes associated with the introduction of the disulfide bond, we crystallized the disulfide mutant in the presence of ADP and IP$_6$ under nonreducing conditions to obtain a structure of IPK1 E82C/S142C (Fig. 5, Table 2). Overall, the structure of IPK1 E82C/S142C was very similar to wild-type IPK1 (root mean squared deviation = 0.5 Å). The presence of the disulfide bond shifted the N-lobe in the mutant structure
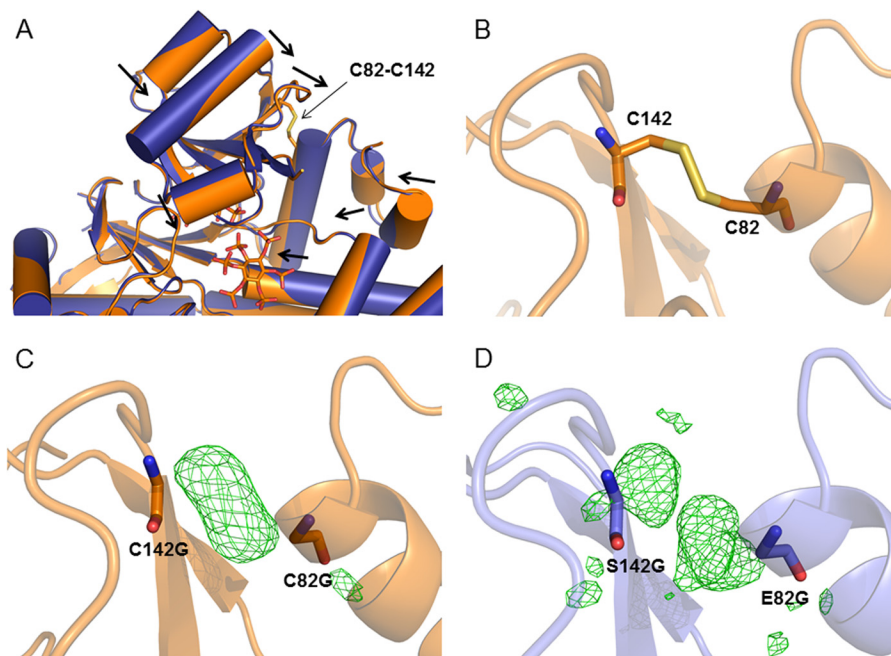
FIGURE 5. **Structure of IPK1 E82C/S142C.** *A*, IPK1 E82C/S142C (Protein Data Bank code: 4LV7) was aligned to wild-type IPK1 (Protein Data Bank code: 3UDZ) using the Dali-Lite Server. A small shift of the N-lobe was observed in the structure of IPK1 E82C/S142C (*orange*) as compared with wild-type IPK1 (*blue*). *Black arrows* indicate movement of the N-lobe. α helices are displayed in *cylindrical form*. The disulfide bond between Cys-82 and Cys-142 is displayed in *stick form*. ADP and IP_6 are shown in *orange, stick form*. *B*, close-up of the disulfide bond between Cys-82 and Cys-142 in the structure of IPK1 E82C/S142C. *C*, refinement of IPK1 E82C/S142C structure with residues Glu-82 and Ser-142 mutated to glycine. $F_o - F_c$ difference map (*green*) is shown at $\sigma = 3.0$. *D*, refinement of wild-type IPK1 structure with residues Glu-82 and Ser-142 mutated to glycine. $F_o - F_c$ difference map (*green*) is shown at $\sigma = 3.0$.

TABLE 2

Data collection and refinement statistics for IPK1 E82C/S142C structure.

Molecular replacement was performed with Protein Data Bank code: 2XAM. One single crystal was used for data collection.

	IPK1 E82C/S142C (PDB ID: 4LV7)
Data collection[a]	
Space group	P1
Cell dimensions	
a, b, c (Å)	59.76, 59.35, 82.23
α, β, γ (°)	83.01, 89.91, 63.41
Wavelength (Å)	1.54178
Resolution (Å)	50.00-2.60 (2.69-2.60)
R_{merge}	0.086 (0.254)
Mean $(I/\sigma I)$	15.4 (4.2)
$I/\sigma I$	3.39 (2.51)
Completeness (%)	94.9 (87.5)
Redundancy (%)	3.9 (3.8)
Refinement	
Resolution (Å)	34.55–2.60
No. of reflections	28,726
R_{work}/R_{free}	0.2244/0.2943
Ramachandran plot (%)[b]	95/4.6/0.4
No. of atoms	6,380
Protein	6,250
Ligand/ion	130
Water	0
B-factors (Å²)	
Protein	33.01
Ligand/ion	25.54
Water	0
r.m.s.[c] deviations	
Bond lengths (Å)	0.022
Bond angles (°)	1.320

[a] Values in parentheses are for highest-resolution shell.
[b] Residues in the favored/allowed/disallowed regions, as determined by MolProbity.
[c] r.m.s., root mean squared.

as compared with the structure of wild-type IPK1 (Fig. 5*A*). Inspection of the electron density indicated the presence of the disulfide bond between Cys-82 and Cys-142 (Fig. 5*B*). To con-

firm the presence of a disulfide bond between these residues, we generated an omit map lacking the side chains at these residues and observed a large unoccupied density in the $F_o - F_c$ map ($\sigma = 3.0$) located between both residues, consistent with the presence of a disulfide bond (Fig. 5*C*). We performed the same refinement using diffraction data from a wild-type structure of IPK1 (Protein Data Bank code: 3UDZ) and did not observe unoccupied density between the two residues in the $F_o - F_c$ difference map ($\sigma = 3.0$), confirming that the density observed is unique to the mutant structure (Fig. 5*D*).

To investigate the effect of the disulfide bond on the overall stability of IPK1, we employed DSF to measure the T_m of wild-type IPK1 and IPK1 E82C/S142C. We compared the T_m values of wild-type IPK1 and IPK1 E82C/S142C in the free state, bound to nucleotide (AMPPNP or ADP) or IP (3,4,5,6-IP_4, IP_5, or IP_6), or in ternary complexes bound to both nucleotide and IP (Fig. 6). We performed this experiment under reducing conditions (with DTT) and nonreducing conditions (without DTT) to detect the effect of the disulfide bond. In the presence or absence of DTT, wild-type IPK1 exhibited similar T_m values as noted above, with the lowest T_m in the apo condition, a slight 2 °C increase in T_m when bound to nucleotide only, a moderate 5 °C increase in T_m when bound to IP only, and a large 12 °C increase in the ternary complex with IP_5 and IP_6 (Fig. 6, first and second sets). AMPPNP + 3,4,5,6-IP_4 failed to stabilize IPK1 to the same extent as AMPPNP + IP_5 and ADP + IP_6 as shown by a 5 °C difference in T_m between the ternary complexes. DTT did not markedly affect any of the T_m values of wild-type IPK1 under any conditions, revealing that the overall stability of wild-type IPK1 is not dependent on disulfide bonds. This is consistent with the structure of wild-type IPK1 that does not have
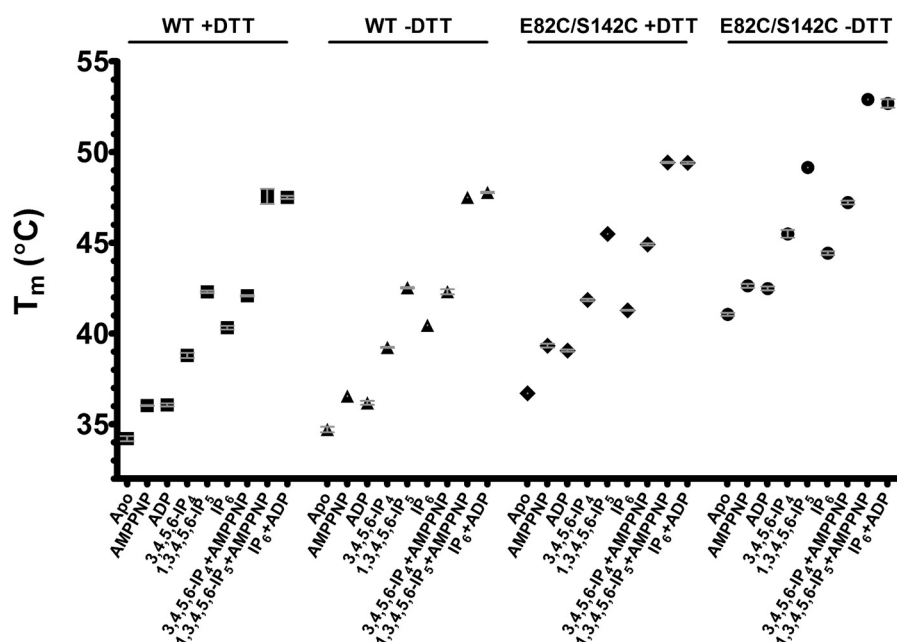
FIGURE 6. **Cys-82-Cys-142 disulfide bond increases overall stability of IPK1.** DSF was performed with wild-type IPK1 or the disulfide mutant IPK1 E82C/S142C in the presence or absence of DTT in complex with different nucleotides and/or inositides as shown. ■, wild-type IPK1 in the presence of DTT (first set); ▲, wild-type IPK1 in the absence of DTT (second set); ◆, IPK1 E82C/S142C in the presence of DTT (third set); ●, IPK1 E82C/S142C in the absence of DTT (fourth set). Each point represents the mean ± S.D. of duplicate experiments. *Error bars* are shown in *gray* for clarity.

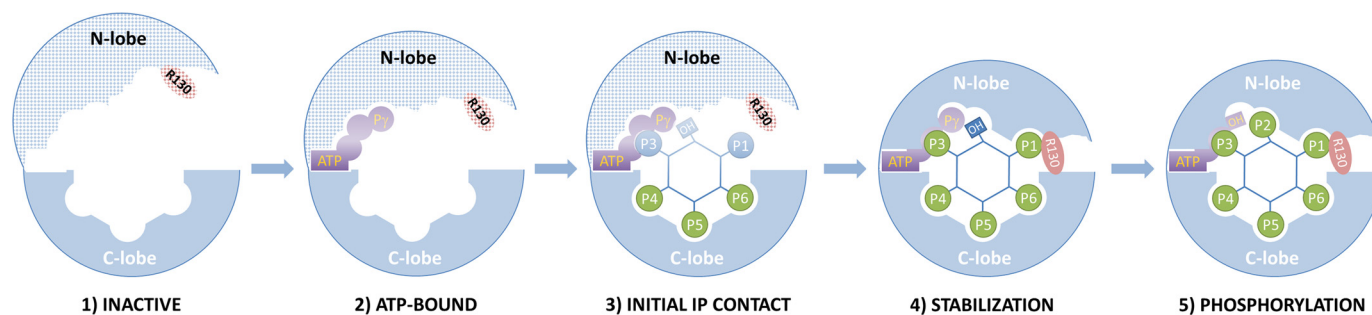FIGURE 7. **Model of IPK1 activation. 1)** In the inactive state, the N-lobe and Arg-130 is labile, and the C-lobe is stable. **2)** Upon ATP binding to both the N-lobe and the C-lobe, the N-lobe is slightly stabilized. **3)** The IP is initially recognized at the 4-, 5-, and 6-positions by the stable C-lobe. **4)** The 1- and 3-position phosphates of the IP induce N-lobe stabilization and the key interaction between Arg-130, and the 1-phosphate stabilizes the N-lobe, resulting in IPK1 activation. **5)** Phosphorylation of the 2′-hydroxyl of IP_5 occurs, forming IP_6.

disulfide bonds. In contrast, IPK1 E82C/S142C exhibited an average increase in T_m of 5.6 °C under each condition as compared with wild-type IPK1 in the absence of DTT, and this increase in T_m is reversible in the presence of DTT, confirming that the disulfide bond is increasing the overall stability of IPK1 (Fig. 6, third and fourth sets). In our kinetic studies, we observed that IPK1 E82C/S142C exhibited increased selectivity for $3,4,5,6-IP_4$ (Table 1). Thus, the engineered disulfide bond that was stabilizing the N-lobe of IPK1 in an IP-independent manner conferred specificity to $3,4,5,6-IP_4$, a poor substrate that lacks the 1-phosphate that is key for N-lobe stabilization, indicating that the stability of the N-lobe is a determinant for substrate specificity of IPK1.

DISCUSSION

Dual roles of the 1- and 3-Phosphates—Here, we investigated the role of the IP phosphates in stabilizing IPK1. We determined that the 1-phosphate is important for localized stability of the N-lobe (Fig. 1), consistent with the IP-free crystal structure of IPK1 that revealed localized destabilization of the region surrounding Arg-130, which interacts with the 1-phosphate (19). We recently investigated specific roles of phosphate groups in binding and activation of IPK1, and we determined that the 5- and 6-phosphates were important for binding of the IP, whereas the 1- and 3-phosphates were important for activation of IPK1 (20). In our current study, we demonstrated that the overall stability of IPK1 is dependent on the N-lobe binding 1- and 3-phosphates (Fig. 2). Thus, the dual roles of the N-lobe binding 1- and 3-phosphates in both IPK1 stabilization and IPK1 activation indicate that the stabilization of the N-lobe is an important component of IPK1 activation. We have also demonstrated that the IP, and not the nucleotide, contributes substantially to the stabilization of the N-lobe of the kinase. This is consistent with our earlier observation that the N-lobe is destabilized in the absence of IP and the structures of Gonzales *et al.* (15), which demonstrated structures bound to IP, but not to nucleotide adopt the stable state (19).

IPK1 Stabilization

Substrate Specificity Is Linked to N-lobe Stability—Changes in protease accessibility and increased protein stability upon substrate binding suggested that activation of IPK1 may be linked to the ability of the IP substrate to stabilize IPK1, so we hypothesized that artificial stabilization of the N-lobe of IPK1 in an IP-independent manner would alter the substrate specificity of IPK1. We engineered the IPK1 E82C/S142C disulfide mutant by introducing a cysteine in the N-lobe of IPK1 at a site that is unstable in the IP-free crystal structure and a second cysteine at a site that is well ordered and apparently stable in all IPK1 crystal structures (Fig. 5) (15, 19). By covalently linking stable and unstable regions, we endeavored to stabilize some or all of the N-lobe. This increase in stability was reflected in our DSF data with IPK1 E82C/S142C, which shows increased T_m values under nonreducing conditions (Fig. 6). This mutant also displays increased selectivity for 3,4,5,6-IP_4 under nonreducing conditions as compared with wild-type IPK1 (Table 1). Given that 3,4,5,6-IP_4 lacks the ability to stabilize wild-type IPK1 as much as IP_5 in ternary complexes (Fig. 1), our data collectively show that substrate specificity is linked to N-lobe stability.

IP-induced Stabilization as a Model of IP Recognition for IPK1—We recently proposed a model for IP recognition wherein interactions with the IP substrate stabilize the N-lobe and C-lobe to promote kinase activation (19). In this model, the stable C-lobe recognizes the 4-, 5-, and 6-phosphates of the IP, and the 1- and 3-phosphates of the IP induce N-lobe stabilization. The key interaction between Arg-130 and the 1-phosphate of the IP stabilizes the N-lobe. Thus, our model possesses a triad of elements that are interconnected for IPK1 activity: 1) substrate specificity, 2) stability, and 3) activation. Our current study provides the necessary evidence for the first time to reconcile all three elements and validates our proposed model. We have linked substrate specificity to kinase stability by demonstrating that IPs possessing the 1-phosphate markedly stabilize the N-lobe as compared with 3,4,5,6-IP_4, which lacks a 1-phosphate, whereas artificial stabilization of the N-lobe of IPK1 alters substrate specificity. We have also found that the 1- and 3-phosphates of the IP provide increased stability to IPK1, whereas the 5- and 6-phosphates do not affect the overall stability of IPK1, consistent with an unstable N-lobe and a stable C-lobe in the absence of IP. Moreover, previous kinetic studies of IPK1 link substrate specificity to kinase activation (20). We contend that IPK1 stability is linked to IPK1 activation because IPK1 stability correlates with the active state in previous crystal structures (19), IPs that display low IPK1 kinase activity (k_{cat}) correlate with a decreased ability to stabilize IPK1 (20), and kinase stability has been validated to be a precursor for activation of PKs, for which IPK1 shares similar features (9, 15). In short, our current data provide strong evidence to support our model that IPK1 substrate specificity is coupled to IPK1 stability and subsequent activation (Fig. 7).

Comparison with PK Activation—Conformational changes that stabilize links between protein kinase N- and C-lobes that occur during activation have been well documented (9). Stabilization of the kinase structure is promoted by the assembly of a hydrophobic spine spanning the two lobes, one of which consists of the Phe residue from the DFG motif, a hydrophobic residue from the αC helix, and two residues buried in the cores
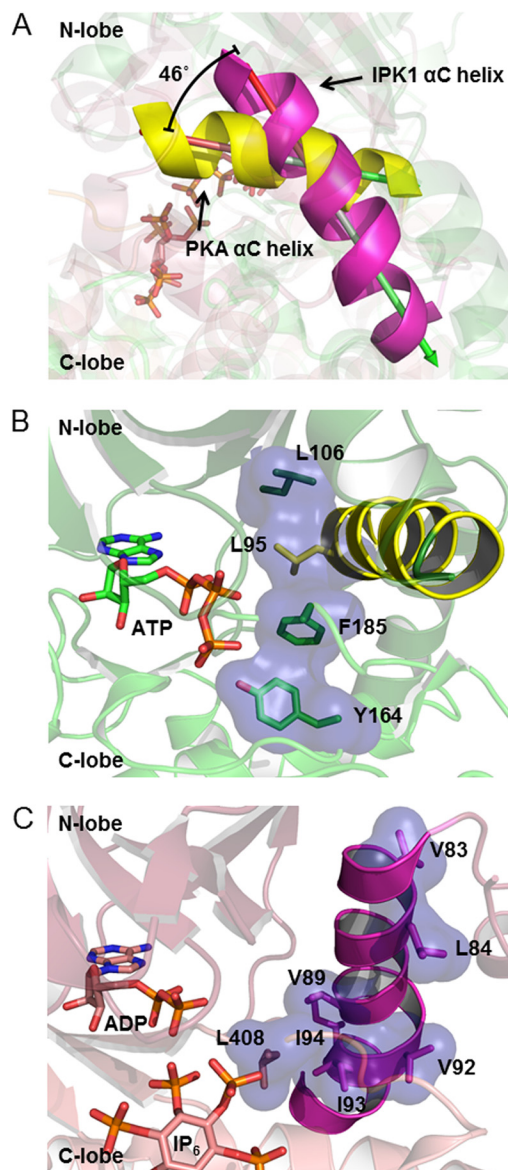

FIGURE 8. **Structural differences between IPK1 and PKA.** Overall alignment between IPK1 (Protein Data Bank code: 3UDZ) and PKA (Protein Data Bank code: 1ATP) was performed with DALI-Lite and yielded a root mean squared deviation = 4.4°. IPK1 is shown in *pink*. PKA is shown in *green*. Both are shown in graphic form. ADP and IP_6 are shown in *pink*, *stick form*. ATP is shown in *green*, *stick form*. The αC helices of IPK1 and PKA are highlighted in *magenta* and *yellow*, respectively. *A*, the angle between the αC helices of IPK1 and PKA was calculated to be 46° using PyMOL (27). *B*, in PKA, the αC helix contributes a hydrophobic residue, Leu-106, to the R-spine (shown in *blue*), a hydrophobic spine that consists of Leu-95, Leu-106, Phe-185, and Tyr-164 and that stabilizes the N-lobe and C-lobe upon activation. *C*, in IPK1, the αC helix orientation precludes any contribution of the hydrophobic residues located on the αC helix (all shown in *stick form*). In addition, a Leu-408 from the DLS motif in IPK1 replaces the bulky Phe-185 of the DFG motif of PKA. Thus, there is no assembly of a hydrophobic spine in IPK1.

of the N- and C-lobes. This structural spine, called the R-spine, assembles only when the DFG and αC helix regulatory motifs sit in their active conformations (8). In IPK1, the αC helix sits at a 46° angle as compared with PKA that precludes the αC helix from contributing a hydrophobic residue to the R-spine (Fig. 8, *A* and *B*). Further, the IPK1 DLS motif lacks the large hydrophobic Phe residue, which likely impairs its ability to assemble a stabilizing R-spine (Fig. 8, *C* and *D*). These structural differ-

ences highlight that IPK1 activation occurs through a different mechanism than found in many PKs. In the proposed model, it is the IP substrate that acts as the bridge between the N-lobe and C-lobe to stabilize the active conformation of the kinase rather than the intrinsic R-spine structure (Fig. 7). The phosphate profile of the IP dictates the ability of the substrate to stabilize the N-lobe of IPK1 and promote kinase activation. This is consistent with previous suggestions that conformational dynamics may play a role in the catalytic cycle of IPK1 (19, 26). Thus, IPK1 retains important features of PK activation such as N- and C-lobe stabilization, yet distinguishes itself from the PKs. These distinct features could be exploited to selectively inhibit IPK1.

Conclusions—In this study, we demonstrate the missing link between IP substrate specificity and the N-lobe stability of IPK1. Our results conclusively support IP-induced stabilization of IPK1 as a proposed model of IP discrimination. IP substrates are very similar, and the elucidation of the unique substrate recognition mechanism of IPK1 among IPKs may provide a basis for selective pharmacological targeting of IPK1. Inhibitors of IPK1 would be useful for ascertaining the functional roles of higher IPs and validation of this IP signaling axis as a therapeutic target.

REFERENCES

1. Sweetman, D., Johnson, S., Caddick, S. E., Hanke, D. E., and Brearley, C. A. (2006) Characterization of an *Arabidopsis* inositol 1,3,4,5,6-pentakisphosphate 2-kinase (AtIPK1). *Biochem. J.* **394,** 95–103

2. Alcázar-Román, A. R., Bolger, T. A., and Wente, S. R. (2010) Control of mRNA export and translation termination by inositol hexakisphosphate requires specific interaction with Gle1. *J. Biol. Chem.* **285,** 16683–16692

3. Shen, X., Xiao, H., Ranallo, R., Wu, W. H., and Wu, C. (2003) Modulation of ATP-dependent chromatin-remodeling complexes by inositol polyphosphates. *Science* **299,** 112–114

4. Agarwal, R., Mumtaz, H., and Ali, N. (2009) Role of inositol polyphosphates in programmed cell death. *Mol. Cell. Biochem.* **328,** 155–165

5. Sarmah, B., Latimer, A. J., Appel, B., and Wente, S. R. (2005) Inositol polyphosphates regulate zebrafish left-right asymmetry. *Dev. Cell* **9,** 133–145

6. Merchant, M. L., Perkins, B. A., Boratyn, G. M., Ficociello, L. H., Wilkey, D. W., Barati, M. T., Bertram, C. C., Page, G. P., Rovin, B. H., Warram, J. H., Krolewski, A. S., and Klein, J. B. (2009) Urinary peptidome may predict renal function decline in type 1 diabetes and microalbuminuria. *J. Am. Soc. Nephrol.* **20,** 2065–2074

7. Verbsky, J., and Majerus, P. (2005) Increased levels of inositol hexakisphosphate (InsP6) protect HEK293 cells from tumor necrosis factor (α)- and Fas-induced apoptosis. *J. Biol. Chem.* **280,** 29263–29268

8. Ten Eyck, L. F., Taylor, S. S., and Kornev, A. P. (2008) Conserved spatial patterns across the protein kinase family. *Biochim. Biophys. Acta* **1784,** 238–243

9. Ubersax, J. A., and Ferrell, J. E., Jr. (2007) Mechanisms of specificity in protein phosphorylation. *Nat. Rev. Mol. Cell Biol.* **8,** 530–541

10. Irvine, R. F., and Schell, M. J. (2001) Back in the water: the return of the inositol phosphates. *Nat. Rev. Mol. Cell Biol.* **2,** 327–338

11. Miller, G. J., and Hurley, J. H. (2004) Crystal structure of the catalytic core of inositol 1,4,5-trisphosphate 3-kinase. *Mol. Cell* **15,** 703–711

12. Holmes, W., and Jogl, G. (2006) Crystal structure of inositol phosphate multikinase 2 and implications for substrate specificity. *J. Biol. Chem.* **281,** 38109–38116

13. Miller, G. J., Wilson, M. P., Majerus, P. W., and Hurley, J. H. (2005) Specificity determinants in inositol polyphosphate synthesis: crystal structure of inositol 1,3,4-trisphosphate 5/6-kinase. *Mol. Cell* **18,** 201–212

14. Wang, H., Falck, J. R., Hall, T. M., and Shears, S. B. (2012) Structural basis for an inositol pyrophosphate kinase surmounting phosphate crowding. *Nat. Chem. Biol.* **8,** 111–116

15. González, B., Baños-Sanz, J. I., Villate, M., Brearley, C. A., and Sanz-Aparicio, J. (2010) Inositol 1,3,4,5,6-pentakisphosphate 2-kinase is a distant IPK member with a singular inositide binding site for axial 2-OH recognition. *Proc. Natl. Acad. Sci. U.S.A.* **107,** 9608–9613

16. Knighton, D. R., Zheng, J. H., Ten Eyck, L. F., Xuong, N. H., Taylor, S. S., and Sowadski, J. M. (1991) Structure of a peptide inhibitor bound to the catalytic subunit of cyclic adenosine monophosphate-dependent protein kinase. *Science* **253,** 414–420

17. Sicheri, F., Moarefi, I., and Kuriyan, J. (1997) Crystal structure of the Src family tyrosine kinase Hck. *Nature* **385,** 602–609

18. Ozkirimli, E., and Post, C. B. (2006) Src kinase activation: A switched electrostatic network. *Protein Sci.* **15,** 1051–1062

19. Gosein, V., Leung, T. F., Krajden, O., and Miller, G. J. (2012) Inositol phosphate-induced stabilization of inositol 1,3,4,5,6-pentakisphosphate 2-kinase and its role in substrate specificity. *Protein Sci.* **21,** 737–742

20. Gosein, V., and Miller, G. J. (2013) Roles of phosphate recognition in inositol 1,3,4,5,6-pentakisphosphate 2-kinase (IPK1) substrate binding and activation. *J. Biol. Chem.* **288,** 26908–26913

21. Schneider, C. A., Rasband, W. S., and Eliceiri, K. W. (2012) NIH Image to ImageJ: 25 years of image analysis. *Nat. Methods* **9,** 671–675

22. Dombkowski, A. A. (2003) Disulfide by Design: a computational method for the rational design of disulfide bonds in proteins. *Bioinformatics* **19,** 1852–1853

23. Otwinowski, Z., and Minor, W. (1997) Processing of x-ray diffraction data collected in oscillation mode. *Methods Enzymol.* **276,** 307–326

24. Adams, P. D., Afonine, P. V., Bunkóczi, G., Chen, V. B., Davis, I. W., Echols, N., Headd, J. J., Hung, L. W., Kapral, G. J., Grosse-Kunstleve, R. W., McCoy, A. J., Moriarty, N. W., Oeffner, R., Read, R. J., Richardson, D. C., Richardson, J. S., Terwilliger, T. C., and Zwart, P. H. (2010) PHENIX: a comprehensive Python-based system for macromolecular structure solution. *Acta Crystallogr. D Biol. Crystallogr.* **66,** 213–221

25. Emsley, P., and Cowtan, K. (2004) Coot: model-building tools for molecular graphics. *Acta Crystallogr. D Biol. Crystallogr.* **60,** 2126–2132

26. Baños-Sanz, J. I., Sanz-Aparicio, J., Whitfield, H., Hamilton, C., Brearley, C. A., and González, B. (2012) Conformational changes in inositol 1,3,4,5,6-pentakisphosphate 2-kinase upon substrate binding: role Of N-terminal lobe and enantiomeric substrate preference. *J. Biol. Chem.* **287,** 29237–29249

27. DeLano, W. L. (2010) *The PyMOL Molecular Graphics System*, version 1.3r1, Schrödinger, LLC, New York